High-pressure structural study of MnF$_2$

Elissaios Stavrou,[1,2,*] Yansun Yao,[3,4] Alexander F. Goncharov,[1,5] Zuzana Konôpková,[6] and Constantine Raptis[7]

[1]*Geophysical Laboratory, Carnegie Institution of Washington, Washington, D.C., USA*
[2]*Lawrence Livermore National Laboratory, Physical and Life Sciences Directorate, P.O. Box 808 L-350, Livermore, California 94550, USA*
[3]*Department of Physics and Engineering Physics, University of Saskatchewan, Saskatoon Saskatchewan, S7N 5E2, Canada*
[4]*Canadian Light Source, Saskatoon, Saskatchewan, S7N 2V3, Canada*
[5]*Key Laboratory of Materials Physics and Center for Energy Matter in Extreme Environments,
Institute of Solid State Physics, Chinese Academy of Sciences, Hefei 230031, China*
[6]*DESY Photon Science, D-22607 Hamburg, Germany*
[7]*Department of Physics, National Technical University of Athens, GR-15780 Athens, Greece*

Manganese fluoride (MnF$_2$) with the tetragonal rutile-type structure has been studied using a synchrotron angle-dispersive powder x-ray diffraction and Raman spectroscopy in a diamond anvil cell up to 60 GPa at room temperature combined with first-principles density functional calculations. The experimental data reveal two pressure-induced structural phase transitions with the following sequence: rutile $\rightarrow$ SrI$_2$ type (3 GPa)$\rightarrow$ α-PbCl$_2$ type (13 GPa). Complete structural information, including interatomic distances, has been determined in the case of MnF$_2$ including the exact structure of the debated first high-pressure phase. First-principles density functional calculations confirm this phase transition sequence, and the two calculated transition pressures are in excellent agreement with the experiment. Lattice dynamics calculations also reproduce the experimental Raman spectra measured for the ambient and high-pressure phases. The results are discussed in line with the possible practical use of rutile-type fluorides in general and specifically MnF$_2$ as a model compound to reveal the HP structural behavior of rutile-type SiO$_2$ (Stishovite).

I. INTRODUCTION

High-pressure phase transitions in the rutile-type (Fig. 1) structured [D$_{4h}^{14}$, S.G. $P4_2/mnm$ (136) $Z = 2$] difluorides [1–4] and oxides [5–8] have attracted considerable interest for several reasons. First, these compounds are archetypal simple ionic solids, making them particularly suitable for testing theoretical approaches [1]. For example, the HP cotunnite-type (PbCl$_2$) structure of TiO$_2$ (rutile) has been proposed [9] as the hardest known oxide. Second, they are isomorphous (at ambient pressure) with the first high pressure form of SiO$_2$ (Stishovite), thus making more achievable the high-pressure transformations [2,10] for the materials of this structural family assuming that the HP phase diagram of these compounds may be analogous to that of SiO$_2$. The high-pressure phase diagram of these compounds appears rich and diverse, with a variety of HP phases (mainly known structural types of AX$_2$ compounds) but there is no well established high pressure structural route. Nevertheless, a typical rutile $\rightarrow$ CaCl$_2$ type [orthorhombic distortion of rutile SG $Pnnm$ (58)] $\rightarrow$ α-PbO$_2$ type [orthorhombic SG $Pbcn$ (60)] $\rightarrow$ CaF$_2$ type [cubic fluorite SG Fm-$3m$ (225)] or PdF$_2$ type (cubic modified fluorite) $\rightarrow$ α-PbCl$_2$ type [cotunnite orthorhombic SG $Pnma$ (62)] sequence of high-pressure phases has been proposed [1,11,12] (see also Ref. [13] for a complete review on AB$_2$ compounds under pressure) with an overall increase in cation coordination number from 6 (rutile) to 9 (cotunnite).

Among various such rutile compounds, MnF$_2$, together with ZnF$_2$, have attracted particular attention, mainly because the ionic radius ratio of cation to anion $R_A/R_X = 0.63$ [14]

is the largest one compared to other members of this crystal class and close to the upper limit (0.732) for a stable rutile structure [12]. Moreover, it has been recently proposed [15] that the high-pressure phases of MnF$_2$ are effective in reducing exciton migration among Mn^{2+}, thus yielding an increased photoluminescence efficiency. Before we refer to the previous high pressure studies on MnF$_2$ it would be useful to discuss the general structural systematics of rutile-type compounds under pressure. We can distinguish two main structural families, namely the rutile and the fluorite family, based on the coordination number and the relative arrangement of the cations and anions. In the first family, except of the prototypical tetragonal rutile where cations are sixfold coordinated and anions threefold, the orthorhombic CaCl$_2$ type (which is a simple distortion of rutile) can also be included. The phase transition from rutile to CaCl$_2$ type has been observed in several rutile-type difluorides and oxides (e.g., Refs. [3,4,7,8]), and it should be ferroelastic and of second order [3,4,7,8]. Moreover, the α-PbO$_2$ type can also be viewed as an orthorhombic distortion of rutile keeping the 6-3 coordination. The second family includes the prototypical cubic fluorite CaF$_2$ type (Fig. 1) where cations form a FCC lattice and anions a simple cubic one (WP 8c 0.25), which results in a 8-4 coordination. Various so-called distorted fluorite structural types can be found in previous studies [12] as high-pressure phases. For instance, PdF$_2$ type and FeS$_2$ type (pyrite) are cubic modifications of fluorite where cations keep the FCC arrangement but the position of anions deviates from the ideal one, resulting in anion-anion bonding in the case of the FeS$_2$ type. It is worth noting that the PdF$_2$ type, although referred to as pyrite type in the literature, represents the structure recently reported [16] as the high-pressure phase of SiO$_2$ above 261 GPa. A very slight orthorhombic distortion of

_____
*stavrou1@llnl.gov

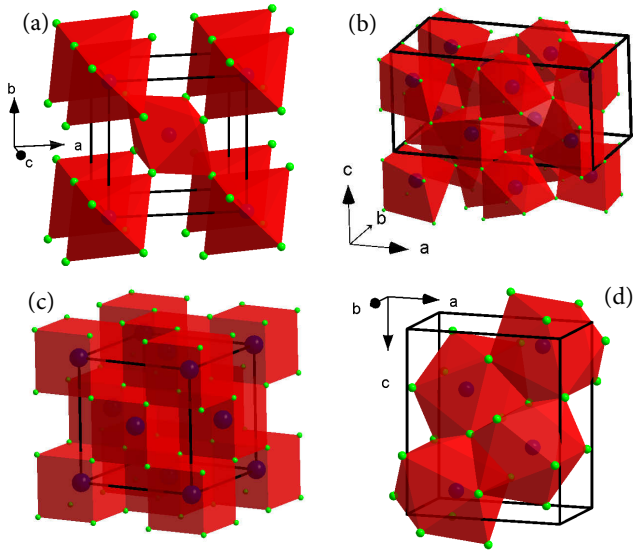FIG. 1. Schematic representations of: (a) rutile-type, (b) SrI_2-type, (c) fluorite, and (d) α-$PbCl_2$-type crystal structures of MnF_2. Blue and green spheres indicate Mn and F anions, respectively.

PdF_2 results in the distorted PdF_2 type (SG 61 *Pbca*) [17]. The coordination of both PdF_2 and distorted PdF_2 type is usually expressed as $(6 + 2) - 4$ indicating the deviation from the 8-4 fluorite. On the other hand, a simple tetragonal distortion of the fluorite, where anions keep the ideal cubic arrangement, results in a tetragonal distorted fluorite structure like, for example, *I4/mmm* [17]. It can be easily understood that there are several different modifications (distortions) of the parent fluorite structure with cubic, tetragonal, or orthorhombic symmetries (see Fig. 1 of Ref. [17]). The exact route of the observed phase transitions for each compound depends on the relative ionic radius ratio, the ionic character of the cation (i.e., existence of *d* electrons in the case of transition metals), and finally the degree of achievable hydrostatic conditions. The latter circumstance represents the more crucial reason for discrepancies between theoretical predictions and experimental findings as has been clearly shown in the case of CoF_2 [17]. This suggests that distinct, although closely related, structures (members of the same family as previously described) may be observed depending on experimental conditions [17].

The high pressure structural behavior of MnF_2 has been extensively studied both theoretically [10] and experimentally [2,12,18–21] during the past three decades. However, a detailed equation of states (EOS) of MnF_2 is not accurately established, and only a few indicative volumes and lattice parameters have been reported at certain pressures up to 25 GPa for static compression [12] and to ≈ 30 GPa for shock compression [18]. A common phase change route can be concluded from the previous studies: Rutile type MnF_2 transforms into a distorted fluorite type at about 3 GPa (depending on experimental conditions) and then into a α-$PbCl_2$ type above 10 GPa. The exact crystal structure of the distorted fluorite phase is still unclear. Yagi *et al.* [2] proposed a tetragonal crystal structure, S.G. *P-42m* (111) $Z = 4$, distinct from any other structural type observed for AB_2 compounds. Other studies [22] also suggested a

tetragonal cell without giving a SG. This has been debated by Smolander [10] based on *ab initio* calculations where an orthorhombic *Aea2*(41) structure, also with $Z = 4$, has been proposed. Moreover, an α-PbO_2 type (distorted rutile) has been observed as a metastable phase upon pressure release after static [19] or shock [18] compression or in a very narrow pressure range (0.7 GPa) between rutile and distorted fluorite structure [12]. The pressure of rutile to α-PbO_2-type phase transition and the pressure stability range of the latter structure strongly depends on hydrostaticity during measurements and crystallinity (single or polycrystalline) of starting material.

In order to address these issues, we have carried out a detailed x-ray powder diffraction, Raman spectroscopy, and computational study of MnF_2 up to 60 GPa. To the best of our knowledge no Raman data have been reported previously for MnF_2 at high pressures. Our results reveal two phase transitions to an orthorhombic structure (HP-I) and to α-$PbCl_2$ type (HP-II) at about 3 GPa and 13 GPa, respectively. The previously debated, HP-I phase is completely characterized, based on structural resemblance with the SrI_2 type, which is found to be a distorted fluoritelike structure distinct from the various previously proposed structures for MnF_2. The pressure stability range of the HP-II phase is very extensive, and MnF_2 remains in this phase up to 60 GPa, which signals the high stability of this phase. In contrast no indication of the α-PbO_2-type phase has been observed. Our first-principles total-energy and lattice-dynamics calculations confirm the experimental findings whereas the calculated equation of state and Raman spectra agree quantitatively with the experimental data. The correlation between MnF_2 and SiO_2 high-pressure phase change routes and the anticipated high-pressure phases of SiO_2 based on the behavior of MnF_2 (as model material) are also discussed.

II. EXPERIMENTAL AND COMPUTATIONAL METHODS

A single crystal of MnF_2 was grounded to fine powder for the angle dispersive x-ray diffraction (XRD) measurements and loaded in a diamond anvil cell (DAC) with neon (Ne) as the pressure transmitting medium (PTM). For the Raman measurements, small chips from the same piece of single crystal were used with Ne as PTM. Small quantities of ruby and gold powder were also loaded for determination of pressure through ruby luminescence [23] and gold EOS, respectively. XRD data were collected at the Extreme Conditions Beamline P02.2 at DESY (Germany) using a Perkin Elmer detector. The monochromatic x-ray beam (wavelength $\lambda = 0.2898$ Å) was focused to a nominal diameter of $4\,\mu$m. The images were integrated using the FIT2D [24] program to yield intensity versus 2θ diagrams. Raman spectra were measured using the 488 nm line from a solid state laser for excitation. An experimental setup capable of recording Raman spectra at very low wave numbers ($\prec 10\,\text{cm}^{-1}$) using solid state notch filters was used.

First-principles calculations were performed using the spin-polarized version of the Vienna *ab initio* simulation package (VASP) [25]. Generalized gradient approximation (GGA) was employed with projected augmented wave (PAW) potentials [26,27] and Perdew-Burke-Ernzerhof (PBE) exchange correlation functional [28]. The wave functions were expanded in a plane-wave basis set with an energy cutoff

of 520 eV. Valence electron configurations of $3d^5\,4s^2$ for Mn atom and $2s^2\,2p^5$ for F atom were employed. Effects of electron correlations beyond the GGA approximation on the Mn d shell were taken into account by employing the GGA+U method together with the simplified rotationally invariant approach [29]. The value of 5.9 eV is used for U_{eff} ($U_{\text{eff}} = U - J$) since it can produce the cell parameters that agree to within 3% with the experimental values. Brillouin zone integrations were carried out using $8 \times 8 \times 12$, $6 \times 6 \times 12$, $8 \times 12 \times 6$, and $12 \times 12 \times 12$ Monkhorst-Pack (MP) meshes [30] for the $P4_2/mnm$, $Pbca$, $Pnma$, and $Fm\text{-}3m$ structures, respectively. In order to correctly describe the magnetic effects, total-energy calculations were tested on three spin configurations, ferromagnetic (FM), antiferromagnetic (AFM), and nonmagnetic (NM), using the $P4_2/mnm$, $Pbca$, $Pnma$, and $Fm\text{-}3m$ structures. Results show that the AFM configuration always yields the lowest energy for all tested structures. This finding agrees very well with the previous theoretical studies on CoF_2 [17] and FeF_2 [31]. The AFM configurations were therefore employed for all total-energy and lattice dynamics calculations. Phonon frequencies at the Brillouin zone center were calculated using the density functional perturbation theory and from which the Raman active modes were identified.

III. RESULTS AND DISCUSSION

A. Structural properties under pressure

Figure 2 shows integrated diffraction patterns of MnF_2 at selected pressures. The evolution of the XRD data shows discontinuous changes at about 3 and 13 GPa, revealing the occurrence of two phase transitions. No sign of other phase transitions has been observed up to the highest pressure of this study (60 GPa). The patterns of the first HP phase resemble the expected (calculated) pattern of the $P\text{-}42m$ structure proposed by Yagi *et al.*, but they reveal the existence of low intensity peaks that cannot be indexed with the $P\text{-}42m$ tetragonal cell. Moreover, the relative Bragg peak intensities are not in good agreement with the expected ones, as was also noted by Yagi *et al.* From our detailed indexing we concluded that a primitive cell with eight formula units, instead of four in $P\text{-}42m$ and $Aea2$, is needed in order to fully index the observed Bragg peaks. The observed Bragg peaks can be very well indexed with an orthorhombic cell with $a = 10.091$ Å, $b = 5.215$ Å, and $c = 5.008$ Å at 7.2 GPa. The corresponding values of the lattice parameters resemble very much the orthorhombic ($oP24$, S.G. $Pbca$ (61) $Z = 8$) phases of SrI_2 (at ambient pressure) and ZrO_2 (at high temperature [32]). This phase has also been proposed by Haines *et al.* [11] as the high pressure modification of α-PbO_2. An almost perfect agreement between the observed and the calculated intensities is obtained using the positional parameters of this phase [11]. This structure can be viewed as a distorted fluorite type with doubling of one axis due to the displacement of cations from the ideal FCC positions (see Fig. 1) forming a sevenfold coordination. This means that this structural type is intermediate between simple cubic or tetragonal distorted fluorite structures (CN $6 + 2$) and fluorite (CN 8). The Bragg peaks of the second HP phase can be very well indexed with the known orthorhombic α-$PbCl_2$-type
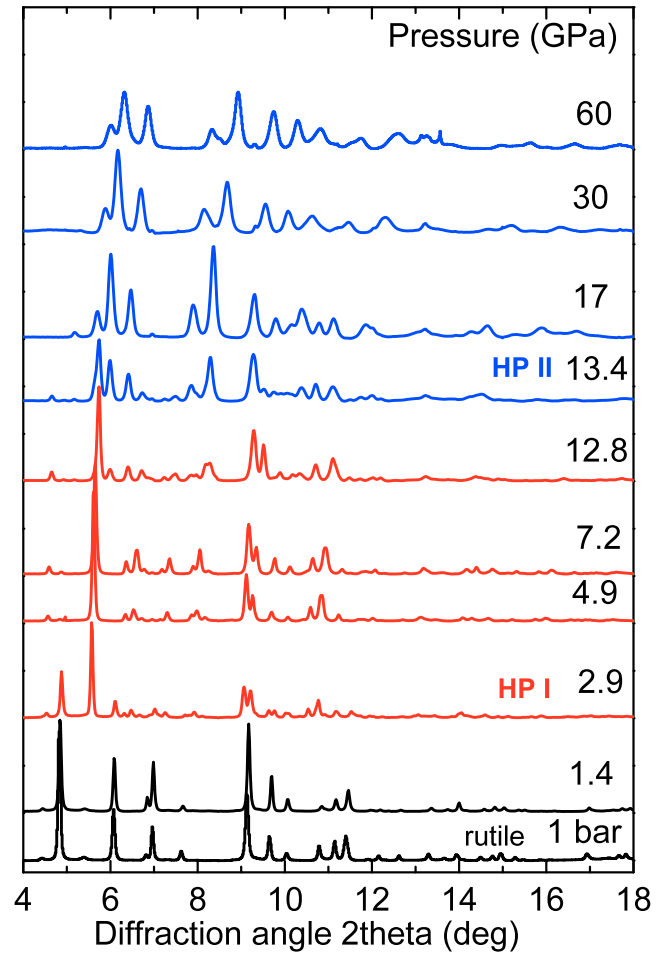

FIG. 2. XRD patterns of MnF_2 at various pressures. The patterns at 2.9 and 13.4 GPa correspond to a phase mixture of rutile-SrI_2 (HP-I) and SrI_2-α-$PbCl_2$ (HP-II) phases.

structure (cotunnite, S.G. $Pnma$ (62) $Z = 4$). No indication of the α-PbO_2 phase has been traced, and MnF_2 remains in rutile type up to 3 GPa where it transforms directly to HP-I. A plausible explanation is that this phase was bypassed due to the very good hydrostatic conditions of the present study, since Ne used as PTM remains liquid up to 4 GPa [33].

To determine the structural parameters the diffraction patterns were analyzed by performing Rietveld refinements using the GSAS [34] software. Typical refined profiles are shown in Fig. 3 for (a) 1.4 GPa, rutile structure, (b) 7.2 GPa, SrI_2 type, and (c) 15 GPa, α-$PbCl_2$ type. The corresponding structural details along with the theoretical values are summarized in Table I. From the XRD data of MnF_2, we have obtained the lattice parameters, the cell volume per formula unit ($V_{p.f.u.}$), and the interatomic distances for the three structures as functions of pressure. The results are compared with the theoretical values shown in Figs. 4 and 5, respectively. The experiment and theory agree very well in the lattice parameters for all three phases. The plots of ($V_{p.f.u.}$) versus pressure (Fig. 4) show a volume reduction of 10.2% (theoretical value: 9.4%) for the rutile to HP-I transition at 3 GPa, and 9.3% (theoretical value: 8.8%) for the HP-I to HP-II one at 13 GPa. Usually, such large volume collapses are indicative of major atomic rearrangements which
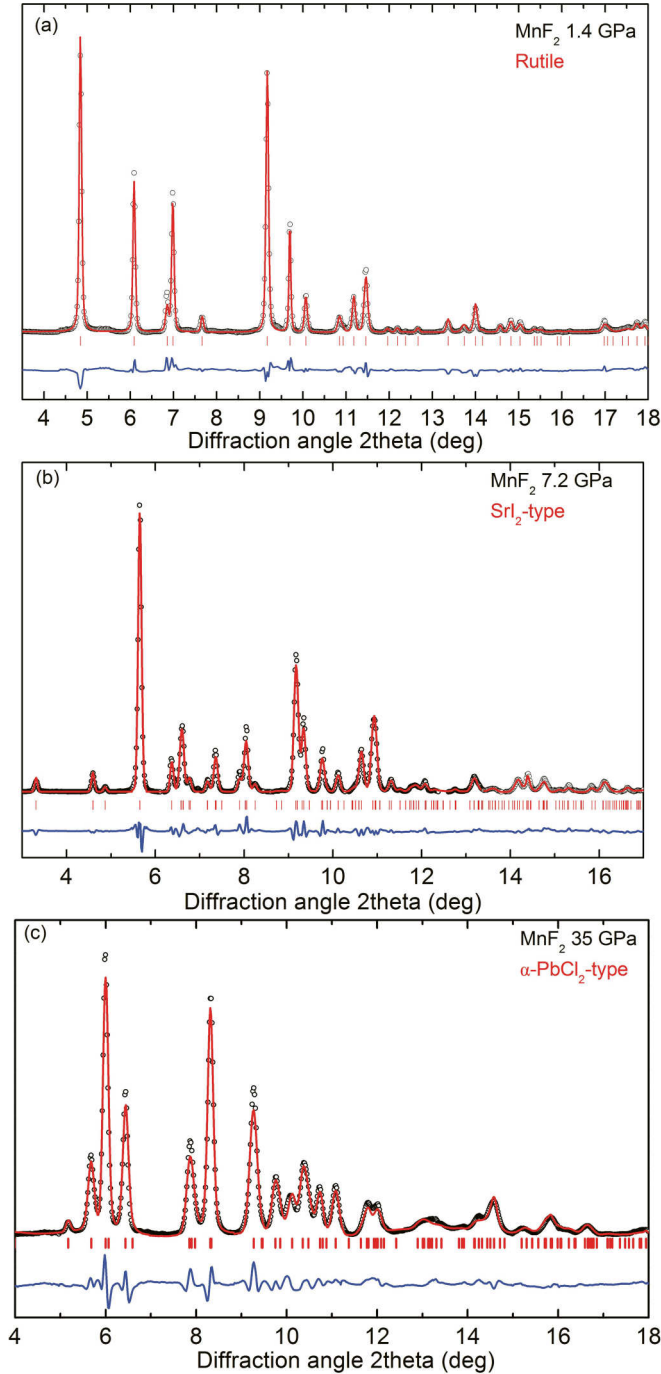
FIG. 3. Rietveld refinement results for MnF_2 at: (a) 1.4 GPa, rutile structure, (b) 7.2 GPa, SrI_2 type, and (c) 33 GPa, α-$PbCl_2$ type. Symbols correspond to the measured profile; the red solid lines represent the results of Rietveld refinements. The difference curves (blue curves) are shown also. Vertical ticks mark positions of Bragg peaks.

parameters obtained in this way are given in Table I. The obtained bulk modulus for rutile structure (98GPa) is in good agreement with previous studies using measurements of sound velocities [36] (88GPa) and XRD [37] (94GPa).

Now we turn our attention to the interatomic distances (Fig. 5) and lattice parameters (Fig. 4) evolution with pressure. From Fig. 4 it can be clearly seen that the *a* axis of the rutile phase is much more compressible (about twice) than the *c* axis in very good agreement with previous findings on other rutile-type difluorides and oxides [37]. It has been proposed [37] that the origin of this anisotropy may be the repulsion of the cations parallel to the *c* axis perpendicular to the edge shearing tetrahedra. From our detailed determination of the interatomic distances, we observe that indeed the short (along the *c* axis, noted as Mn-Mn I) Mn-Mn distance remains almost unchanged with pressure in contrast to the long (between corner and center atoms, noted as Mn-Mn II) which is clearly affected by pressure. Moreover, the four equatorial Mn-F distances (noted as Mn-F II) remain almost constant (following the constant Mn-Mn I distance) in contrast to the two very compressible axial Mn-F distances (noted as Mn-F I). The evolution of the theoretical Mn-F I distances also shows the same trend of decreasing under pressure, but they are less compressible compared with the experimental values. The net effect of these observations is the increase of the distortion of the octahedra which explains the mechanism of the increase of the coordination number. In the case of HP-I we observe a smooth variation (decrease) of the seven different Mn-F distances with increasing pressure. On the other hand, the Mn-Mn distances show a very interesting trend. In the SrI_2-type structure, each Mn^{2+} cation has 12 closest Mn^{2+} neighbors, an equal number with FCC fluorite structure, although not equal with each other. More specifically, we observe seven different distances within the range of ≈ 0.6 Å at 4.9 GPa. From Fig. 5, it can be clearly seen that with increasing pressure, there is an apparent decrease of this range (≈ 0.4 Å at 12.8 GPa) and all distances approach a mean value very close to the expected one (12 equals ones) for a fluorite structure with the same volume (red dashed line in Fig. 5). It is plausible to assume that with higher temperature this distortion may be altered and a perfect FCC sublattice (fluorite or cubic PdF_2) may be formed. Indeed, a cubic fluorite-type structure for MnF_2 has been reported [19] at moderate temperature (> 200 °C). In the case of cotunnite structure, Mn^{2+} cations are ninefold coordinated by F^- anions with seven short and two (equal) longer distances of ≈ 2.7 Å [Fig. 5(b)]. As in the case of SrI_2-type structure, Mn^{2+} cations have 12 closer Mn^{2+} neighbors with five different distances: four with multiplicity 2 and one [noted in Fig. 5(a)] with 4. A smooth decease with pressure for all distances, except the longer Mn-F which remains almost constant, can be seen from Fig. 5.

Concerning the slight discrepancies between experimental and theoretical values of the interatomic distances, the comments are as follows: (a) Although we started with an almost perfect powder substance and consequently with a uniform intensity ringlike 2D XRD image, this has been, normally, partially altered (spottylike) after the first phase transition, thus, introducing an experimental error in the determination of the positional parameters. (b) In principle, the *U* parameters in the GGA+*U* calculations should change with both the pressure and the structure. However, using different

in this case involve the change of the coordination number from 6 to 7 and from 7 to 9. We have fitted the experimental pressure-volume data to a third-order Birch-Murnaghan equation of state [35] and determined the bulk modulus *B* and its first derivative *B′* at zero pressure for the rutile and at the experimental onset pressure for the two HP phases. The elastic

TABLE I. Experimental and theoretical structural parameters of rutile, SrI₂-, and α-PbCl₂-type structure of MnF₂ at selected pressures: space group (SG), number of formula units in the unit cell Z, lattice parameters, cell volume per formula unit, bulk modulus B, and its pressure derivative B', Wyckoff site, and the corresponding coordinates. Theoretical values are presented under the experimental values.

P (GPa)	SG	Z	a (Å)	b (Å)	c (Å)	V_{pfu} (Å³)	B (GPa)	B'	WP	x	y	z
0	$P4_2/mnm$	2	4.872(1)	4.872(1)	3.309(1)	39.28(1)	99(2)	4	Mn(2a)	0	0	0
									F(4f)	0.3132(5)	0.3132(5)	0
			4.9153	4.9153	3.320	40.11				0.304	0.304	0
1.45	$P4_2/mnm$	2	4.843(1)	4.843(1)	3.299(1)	38.69(1)			Mn(2a)	0	0	0
									F(4f)	0.297(1)	0.297(1)	0
			4.8755	4.8755	3.3200	39.45				0.3034	0.3034	0
7.2	$Pbca$	8	10.092(3)	5.215(2)	5.008(2)	33.08(3)	118(4)	4	Mn(8c)	0.879(1)	0.039(1)	0.275(1)
			10.097	5.272	5.102	33.945				0.884	0.034	0.267
									F(8c)	0.789(3)	0.341(3)	0.150(2)
										0.794	0.381	0.146
									F(8c)	0.980(4)	0.754(3)	0.480(3)
										0.972	0.737	0.501
33	$Pnma$	4	5.239(3)	3.140(2)	6.249(4)	25.71(8)	148(6)	6	Mn(4c)	0.211(2)	0.25	0.402(2)
			5.318	3.189	6.311	26.76				0.248	0.25	0.379
									F(4c)	0.502(5)	0.25	0.852(4)
										0.527	0.25	0.831
									F(4c)	0.122(5)	0.25	0.064(6)
										0.145	0.25	0.069

U parameters for different structures would result in a change of the energy levels which hinders the enthalpy comparison. The U parameters, as determined at ambient pressure using the rutile structure, may become less accurate at high pressures, and this may be one of the reasons why calculations do not reproduce exactly the interatomic distances for HP phases.

The calculated enthalpies as functions of pressure for the rutile, SrI₂ type, and α-PbCl₂ type of MnF₂ are shown in Fig. 6 over the pressure range 0–25 GPa. At ambient pressure, the calculation correctly reveals the rutile structure as the thermodynamic ground state of MnF₂. The SrI₂-type structure becomes more stable than the rutile structure at ca. 4.2 GPa,

which agrees well with the measured transition pressure of 3 GPa. At 13.1 GPa, the α-PbCl₂-type structure replaces the SrI₂-type structure, consistent with the measured transition at 13 GPa. Along the way, we also examined the two previously proposed structures for HP-I, namely the P-$42m$ structure [2] and the $Aea2$ structure [10]. Interestingly, if we fully optimize these two structures, they both become immediately unstable and transform directly to the fluorite structure. This finding further validates the SrI₂-type structure as the correct HP-I. The enthalpy of the fluorite structure (Fm-$3m$) is presented in Fig. 6 for a comparison.

B. Raman scattering under pressure

Four Raman-active zone-center modes are predicted from group theory for the rutile-type structure with the symmetries: $B_{1g} + E_g + A_{1g} + B_{2g}$. At ambient pressure inside the DAC we observe three, $E_g + A_{1g} + B_{2g}$, out of four expected modes (Fig. 7). The fourth low frequency, expected at c.a. 61 cm⁻¹ [38], Raman mode (of B_{1g} symmetry) is not evident in our spectra; presumably, it is too weak for detection [38]. The Raman frequencies of the observed Raman modes are in excellent agreement with previous studies [38]. The calculated frequencies for the B_{2g}, A_{1g}, and E_g modes are 463 cm⁻¹, 350 cm⁻¹, and 233 cm⁻¹, respectively, which compare well with the experimental values of 457 cm⁻¹, 340 cm⁻¹, and 245 cm⁻¹. The calculated frequency for the missing B_{1g} mode is 72 cm⁻¹. The Raman spectrum of MnF₂ at 4 GPa (Fig. 7) is drastically changed confirming the phase transition observed also by XRD measurements. We would like to point out that analysis of Raman spectra has been hindered by the intense luminescence exhibited by MnF₂ above the first phase transition [15], and this is probably the reason for no reported Raman data under pressure. The appearance of multiple Raman modes strongly indicates that HP-I has a larger and lower symmetry
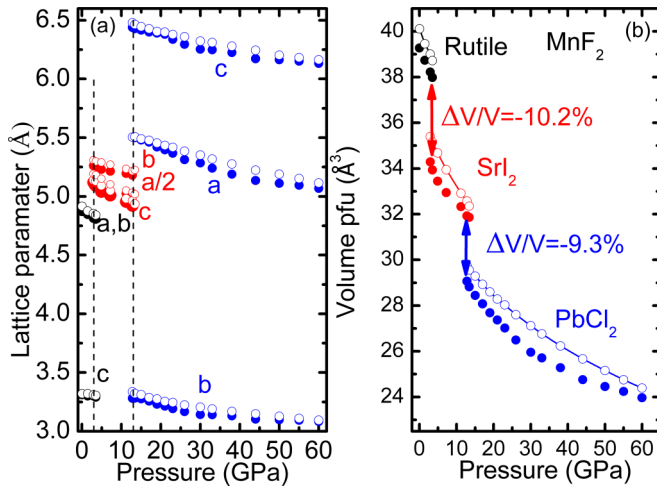

FIG. 4. (a) Pressure dependence of the lattice parameters of MnF₂ and (b) volume-pressure data for the rutile, SrI₂ type and α-PbCl₂ type of MnF₂. Experimental and calculated values are shown with solid and open symbols, respectively.
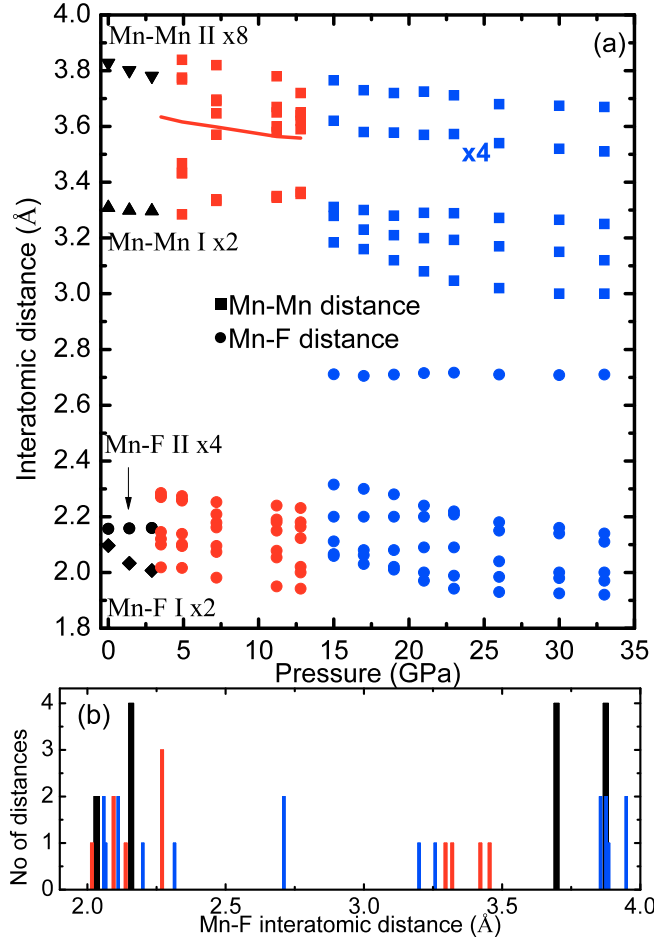
FIG. 5. (a) Selected interatomic distances for the rutile, SrI$_2$ type, and α-PbCl$_2$ type of MnF$_2$ as a function of pressure shown with black, red, and blue symbols, respectively; Mn-F and Mn-Mn distances are noted with solid squares and circles, respectively, for the two high pressure phases. (b) Bar diagram of the various Mn-F distances up to 4 Å for the three different phases of MnF$_2$; distances with very close values are grouped together for clarity. See text for details.

cell in relation to the rutile type. This is in agreement with the proposed orthorhombic SrI$_2$-type ($Z = 8$ vs 2 for rutile) structure as determined by the XRD measurements. Group theory predicts 36 Raman-active zone-center modes with the symmetries: $9A_g + 9B_{1g} + 9B_{2g} + 9B_{3g}$. At least 16 Raman modes can be observed in the 4 GPa Raman spectrum.

Raman spectra at 30 and 40 GPa reveal the existence of the second high-pressure phase HP-II at these pressures. The relatively simpler Raman spectrum suggests a smaller cell in comparison to the SrI$_2$ type. Indeed cotunnite structure determined from XRD has a smaller unit cell ($Z = 4$ vs 8 for SrI$_2$ type). Group theory predicts 18 zone-center Raman active modes: $6A_g + 3B_{1g} + 6B_{2g} + 3B_{3g}$ from which 12 can be observed in the 30 and 40 GPa Raman spectra. In order to perform a tentative assignment we use the theoretical results of a recent [17] combined experimental and theoretical study on the lattice dynamics of CoF$_2$ under pressure which transform to the cotunnite structure at $\approx$45 GPa. To the best of our knowledge there is no other HP Raman study of cotunnite-type fluorides. Moreover, only one Raman peak of CoF$_2$ cotunnite
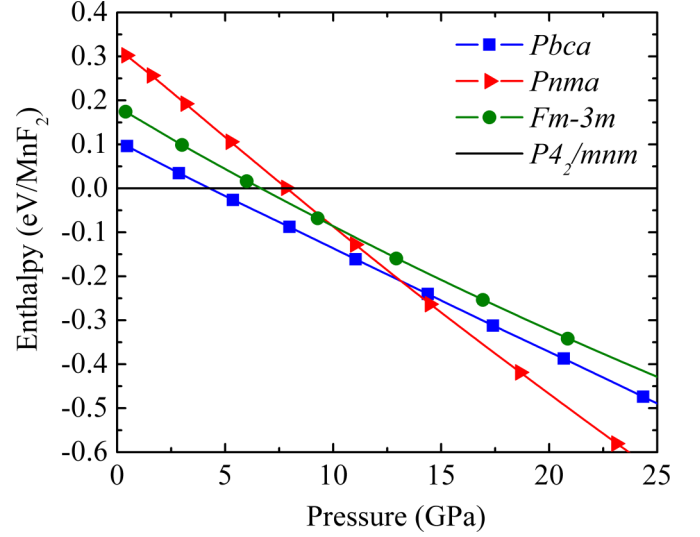

FIG. 6. Calculated enthalpy differences for the rutile, fluorite, SrI$_2$-type, and α-PbCl$_2$-type phases of MnF$_2$ as a function of pressure. The enthalpy of the rutile phase is taken as the reference.
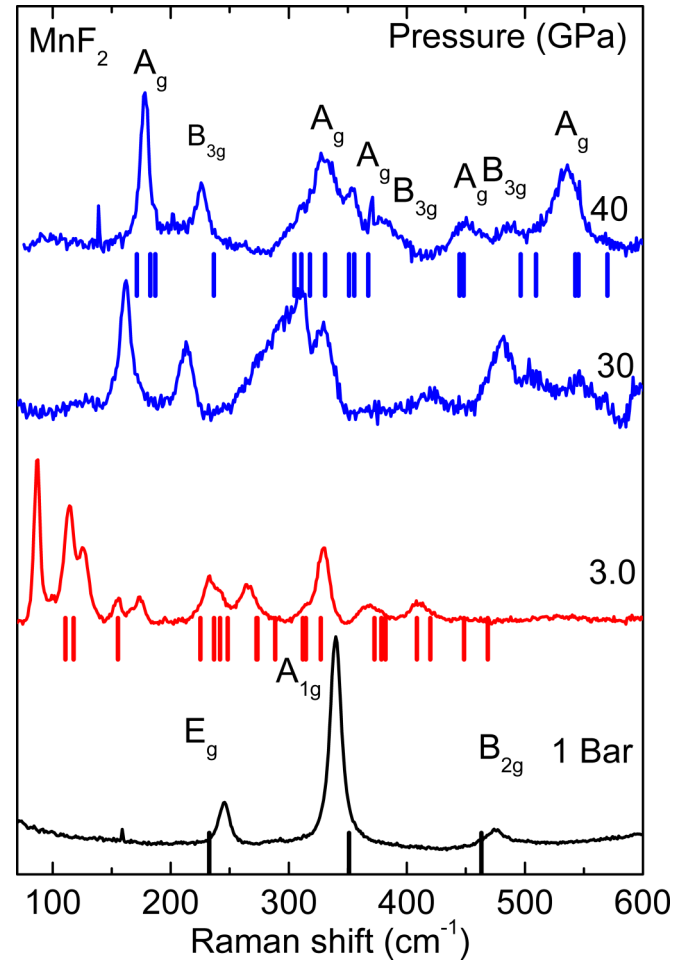

FIG. 7. Raman spectra of MnF$_2$ at various pressures. The black, red, and blue vertical ticks mark the calculated frequency of the Raman peaks for rutile, SrI$_2$-type, and α-PbCl$_2$-type phases of MnF$_2$, respectively.

phase has been observed by Barreda *et al.* [17]. A negligible effect of different mass between Mn and Co is expected at these pressures. The results of the assignment are shown in Fig. 7.

IV. RELATION BETWEEN MnF₂ AND SiO₂ HIGH PRESSURE PHASE DIAGRAMS

As already mentioned, one of the main reasons for the interest in the high pressure structural behavior of rutile structure fluorides is the use of such compounds as model materials for the pressure induced phase transitions of SiO₂. A direct comparison between the phase diagrams is not straightforward for three main reasons: (a) the difference between bonding schemes of oxides and fluorides, (b) hydrostaticity is poorer at higher, at least an order of magnitude, critical pressures in the case of SiO₂, and (c) experimental observations of high pressure forms of SiO₂ are usually combined with applications of high temperature in order to overcome the kinetic barriers. The latter case is of key importance since temperature critically affects the actual structure observed at high pressures. For instance, the SrI₂-type structure of MnF₂ observed in this study is expected to transform to a higher symmetry fluorite structure at temperatures of few hundreds °C. That being said, we believe that a lack or not of a one-to-one structural correspondence is not sufficient to judge whether a model compound is suitable [20]. Instead, here we focus on the structural families, based on the coordination number and cation arrangement, as described in the introduction. Figure 8 shows a bar diagram with the critical pressures and the structural types observed for MnF₂ in this study and SiO₂ from previous experimental [16,39,40] and theoretical [41] studies. The various structural types of rutile family are noted with different colors. The, post-pyrite, cotunnite structure of SiO₂, although not experimentally observed yet, has been predicted [41] as the more stable structure above c.a. 730 GPa. It can be clearly seen that the high-pressure structural behaviors of MnF₂ and SiO₂ fit perfectly not only on the phase sequence but also on the pressure range of relative stability of each family. Although, to the best of our knowledge,there is no prediction of a stable SiO₂ phase above cotunnite, it is plausible to assume that the stability range of this phase extends to at least 2 TPa. However, the actual phase which will be observed in future experiments may deviate from cotunnite for the already mentioned above reasons: (a) bonding schemes, (b) hydrostaticity, and (c) temperature.

V. SUMMARY

The high-pressure phase transition sequence of MnF₂ has been explored by a combined experimental and first-principles study up to 60 GPa. The exact crystal structure of the intermediate phase (HP-I) is fully identified and characterized as SrI₂-type orthorhombic that is distinct from all previously proposed structures. A full structural analysis has been performed including the detailed determination of the various interatomic distances under pressure which allows a better understanding of the mechanisms of the phase transitions. It is noteworthy that, through the series of the observed phase transitions, the coordination number of manganese increases
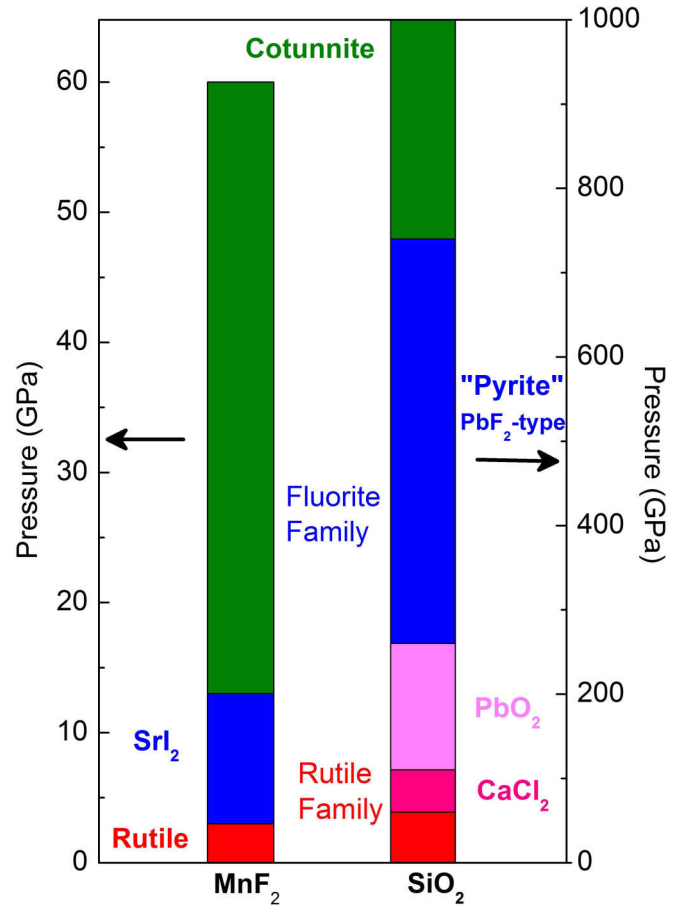

FIG. 8. Bar diagram showing the pressure stability intervals of the different structural modifications of MnF₂ and SiO₂. Critical pressures values are obtained with XRD from this study for MnF₂ and XRD results or theoretical predictions for SiO₂ (see the references given in the text).

from six- (rutile) to seven- (modified fluorite) and finally to ninefold (cotunnite). Given the similarities between the HP phase diagram of MnF₂ and SiO₂, a cotunnite-type (HP-II) ninefold structure can be proposed as the highly anticipated post-pyrite [16] SiO₂ structure.

[1] J. Haines, J. M. Leger, F. Gorelli, D. D. Klug, J. S. Tse, and Z. Q. Li, Phys. Rev. B **64**, 134110 (2001).

[2] T. Yagi and J. Jamieson, J. C. Jamieson, J. Geophys. Res. **84**, 1113 (1979).

[3] A. Perakis, D. Lampakis, Y. C. Boulmetis, and C. Raptis, Phys. Rev. B **72**, 144108 (2005).

[4] I. S. Zouboulis, F. Jiang, J. Wang, and T. S. Duffy, J. Phys. Chem. Solids **75**, 136 (2014).

[5] J. Haines, J. M. Leger, C. Chateau, R. Bini, and L. Ulivi, Phys. Rev. B **58**, R2909 (1998).

[6] J. Haines, J. M. Léger, and O. Schulte, Science **271**, 629 (1996).

[7] J. Haines, J. M. Leger, and S. Hoyau, J. Phys. Chem. Solids **56**, 965 (1995).

[8] H. Hellwig, A. F. Goncharov, E. Gregoryanz, H.-k. Mao, and R. J. Hemley, Phys. Rev. B **67**, 174110 (2003).

[9] L. S. Dubrovinsky, N. A. Dubrovinskaia, V. Swamy, J. Muscat, N. M. Harrison, R. Ahuja, B. Holm, and B. Johansson, Nature (London) **410**, 653 (2001).

[10] K. Smolander, Phys. Scr. **25**, 425 (1982).

[11] J. Haines, J. M. Leger, and O. Schulte, J. Phys.: Condens. Matter **8**, 1631 (1996).

[12] L. Ming, M. Manghnani, T. Matsui, and J. Jamieson, Phys. Earth Planet. Inter. **23**, 276 (1980).

[13] J. M. Leger and J. Haines, Eur. J. Solid State Inorg. Chem. **34**, 785 (1997).

[14] R. D. Shannon, Acta Crystallogr. Sect. A **32**, 751 (1976).

[15] I. Hernandez, F. Rodriguez, and H. D. Hochheimer, Phys. Rev. Lett. **99**, 027403 (2007).

[16] Y. Kuwayama, K. Hirose, N. Sata, and Y. Ohishi, Science **309**, 923 (2005).

[17] J. A. Barreda-Argüeso, S. López-Moreno, M. N. Sanz-Ortiz, F. Aguado, R. Valiente, J. González, F. Rodríguez, A. H. Romero, A. Muñoz, L. Nataf, and F. Baudelet, Phys. Rev. B **88**, 214108 (2013).

[18] T. Hongo, K. G. Nakamura, T. Atou, M. Kikuchi, K. Yubuta, S. Itoh, K. Kusaba, K. Fukuoka, and K.-I. Kondo, Phys. Rev. B **76**, 104114 (2007).

[19] S. S. Kabalkina, L. F. Vereshchagin, and L. M. Lityagina, Sov. Phys. JETP **29**, 803 (1969).

[20] M. Yamaguchi, T. Yagi, N. Hamaya, and T. Yagi, J. Phys. Soc. Jpn. **61**, 3883 (1992).

[21] L. M. Azzaria and F. Dachille, J. Phys. Chem. **65**, 889 (1961).

[22] L. F. Vereshchagin, S. S. Kabalkina, and A. A. Kotilevets, Sov. Phys. JETP **22**, 1181 (1966).

[23] K. Syassen, High Press. Res. **28**, 75 (2008).

[24] A. P. Hammersley, S. O. Svensson, M. Hanfland, A. N. Fitch, and D. Hausermann, High Press. Res. **14**, 235 (1996), 4th Workshop of the IUCr High Pressure Group on Synchrotron and Neutron Sources, KEK, JAPAN, MAR 22–24, 1995 .

[25] G. Kresse and J. Furthmuller, Phys. Rev. B **54**, 11169 (1996).

[26] G. Kresse and D. Joubert, Phys. Rev. B **59**, 1758 (1999).

[27] P. E. Blöchl, Phys. Rev. B **50**, 17953 (1994).

[28] J. P. Perdew, K. Burke, and M. Ernzerhof, Phys. Rev. Lett. **77**, 3865 (1996).

[29] S. L. Dudarev, G. A. Botton, S. Y. Savrasov, C. J. Humphreys, and A. P. Sutton, Phys. Rev. B **57**, 1505 (1998).

[30] H. Monkhorst and J. Pack, Phys. Rev. B **13**, 5188 (1976).

[31] S. López-Moreno, A. H. Romero, J. Mejía-López, A. Muñoz, and I. V. Roshchin, Phys. Rev. B **85**, 134110 (2012).

[32] O. Ohtaka, T. Yamanaka, S. Kume, N. Hara, H. Asano, and F. Izumi, Proc. Jpn. Acad., Ser. B **66**, 193 (1990).

[33] R. M. Hazen, H. K. Mao, L. W. Finger, and P. M. Bell, Carnegie Ins. Washington Yearb. **79**, 348 (1980).

[34] A. C. Larson and R. B. V. Dreele, GSAS: General Structure Analysis System Report LAUR 86-748, Tech. Rep. (Los Alamos National Laboratory, 2000).

[35] F. Birch, J. Geophys. Res. **83**, 1257 (1978).

[36] D. Gerlich, S. Hart, and D. Whittal, Phys. Rev. B **29**, 2142 (1984).

[37] R. M. Hazen and L. Finger, J. Phys. Chem. Solids **42**, 143 (1981).

[38] S. P. S. Porto, P. A. Fleury, and T. C. Damen, Phys. Rev. **154**, 522 (1967).

[39] K. J. Kingma, R. E. Cohen, R. J. Hemley, and H. K. Mao, Nature (London) **374**, 243 (1995).

[40] L. S. Dubrovinsky, S. K. Saxena, P. Lazor, R. Ahuja, O. Eriksson, J. M. Wills, and B. Johansson, Nature (London) **388**, 362 (1997).

[41] A. R. Oganov, M. J. Gillan, and G. D. Price, Phys. Rev. B **71**, 064104 (2005).